Electronic Supporting Information

Design of a Three-state Switchable Chromogenic Radical-based Moiety and Its Translation to Molecular Logic Systems

Sanjoy Mukherjee [a] and Bryan W. Boudouris [a,b,*]

[a] Charles D. Davidson School of Chemical Engineering and [b] Department of Chemistry, Purdue University, West Lafayette, IN-47907, USA. Email: boudouris@purdue.edu

Materials

All reagents were purchased from Sigma-Aldrich, and they were used as received unless otherwise specified. 2,6-di-tert-butyl-4-((3,5-di-tert-butyl-4-hydroxyphenyl) (4-vinylphenyl)methylene) cyclohexa -2,5-dien-1-one (GStH) was prepared according to a previously reported procedure available in literature.[1]

General Methods

Ultraviolet–Visible (UV-Vis) light absorption spectroscopy data were acquired on a Cary 60 spectrometer over a wavelength range of $300 \leq \lambda \leq 800$ nm. All the UV-Vis absorption experiments were performed in THF-Water (1:9) mixture as it is moderately good solvent for the materials, inert towards bases (e.g., aq. NaOH), oxidants (e.g., aq. $K_3[Fe(CN)_6]$) or antioxidants (e.g., ascorbic acid); and THF does not inherently act as a base (unlike DMF etc.) towards the phenolic species (GStH and PGStH). Size exclusion chromatography (SEC) data were collected by dissolving the sample at a concentration of 10 mg mL^{-1} in tetrahydrofuran (THF), and these samples were injected into a Hewlett-Packard 1260 Infinity series SEC column equipped with a HP G1362A refractive index (RI) detector. Specifically, the polymers were eluted (with THF serving as the mobile phase) at a volumetric flow rate of 1 mL min^{-1} through three PLgel 5 μm MIXED-C columns maintained at 40 °C. Polystyrene standards (Agilent) of well-defined molecular weight and with narrow molecular weight distributions were used for molecular weight calibrations. ^{1}H NMR (300 MHz) for GStH and PGStH (5 mg mL^{-1}) were recorded on a Bruker ARX300 MHz NMR spectrometer. All solution ^{1}H NMR spectra were referenced internally to the solvent ($CDCl_3$) signal.

Computational Methods

All of the density functional theory (DFT) calculations were performed using standard computational methods and basis sets as incorporated in the Gaussian 09 software package. [2] The most commonly used B3LYP functional, with 6-31G(d) basis sets for all the atoms was used in this regard. Frequency tests of the optimized structures were performed to ascertain stationary points. Time-dependent DFT (TD-DFT) 1st excited state geometry optimizations were performed using only the B3LYP/6-31G(d) methodology (i.e., RB3LYP). The neutral and anionic systems (e.g., GStH and GStB) were optimized using close-shell methods. However, for the GSt, open-shell calculations (i.e., using UB3LYP) were performed. The structure of the polymer was optimized using MM2 method, as incorporated in Chem3D 15.1 software package.

Synthesis of PGStH

To a 5.0 ml dry toluene solution of the monomer, GStH (200 mg), AIBN (5.0 mg, 30.5 µmol), was added and the mixture was stirred for 24 h at 75°C under a nitrogen atmosphere. The polymerization mixture was poured into hexane, and the precipitate was purified via re-precipitation from dichloromethane into hexane to afford the orange powder of PGStH (yield 80%). $M_n = 4.1 \times 10^3$ kg mol^{-1}, $M_w/M_n = 1.2$.

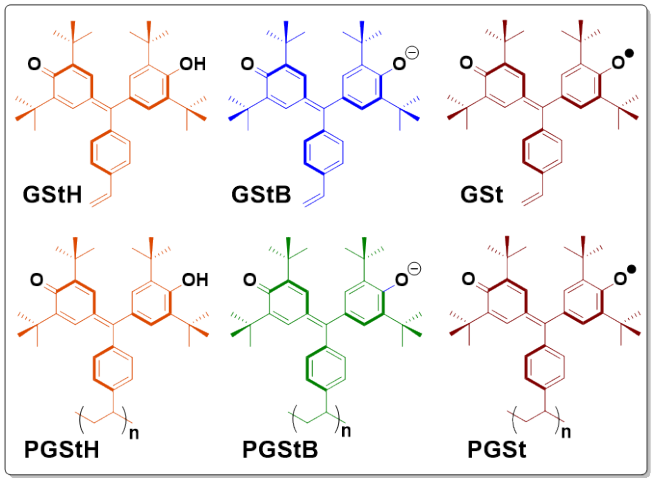

Scheme S1: Molecular formulae of GSt, GStH and GStB (top). Similarly, the same structures for the polymeric systems (PGSt, PGStH and PGStB) are shown in the lower portion of the figure. The colors represent the visual appearances of the entities.

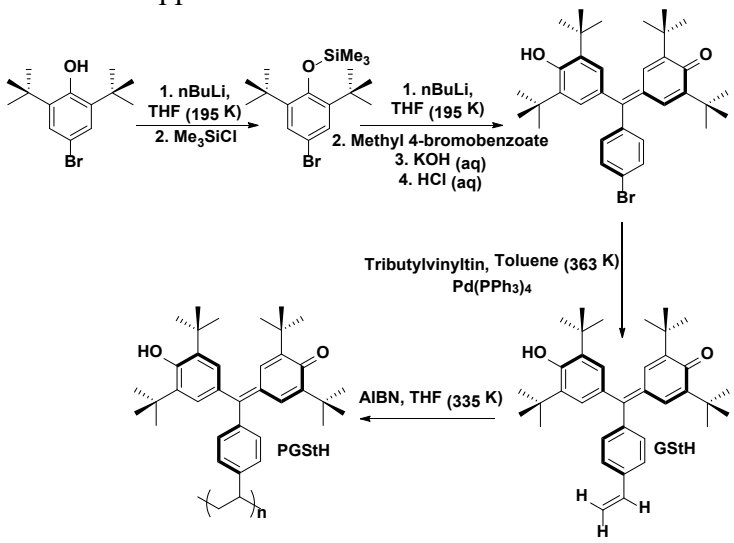

Scheme S2: Synthetic procedure for the preparation of GStH and PGStH.[1]

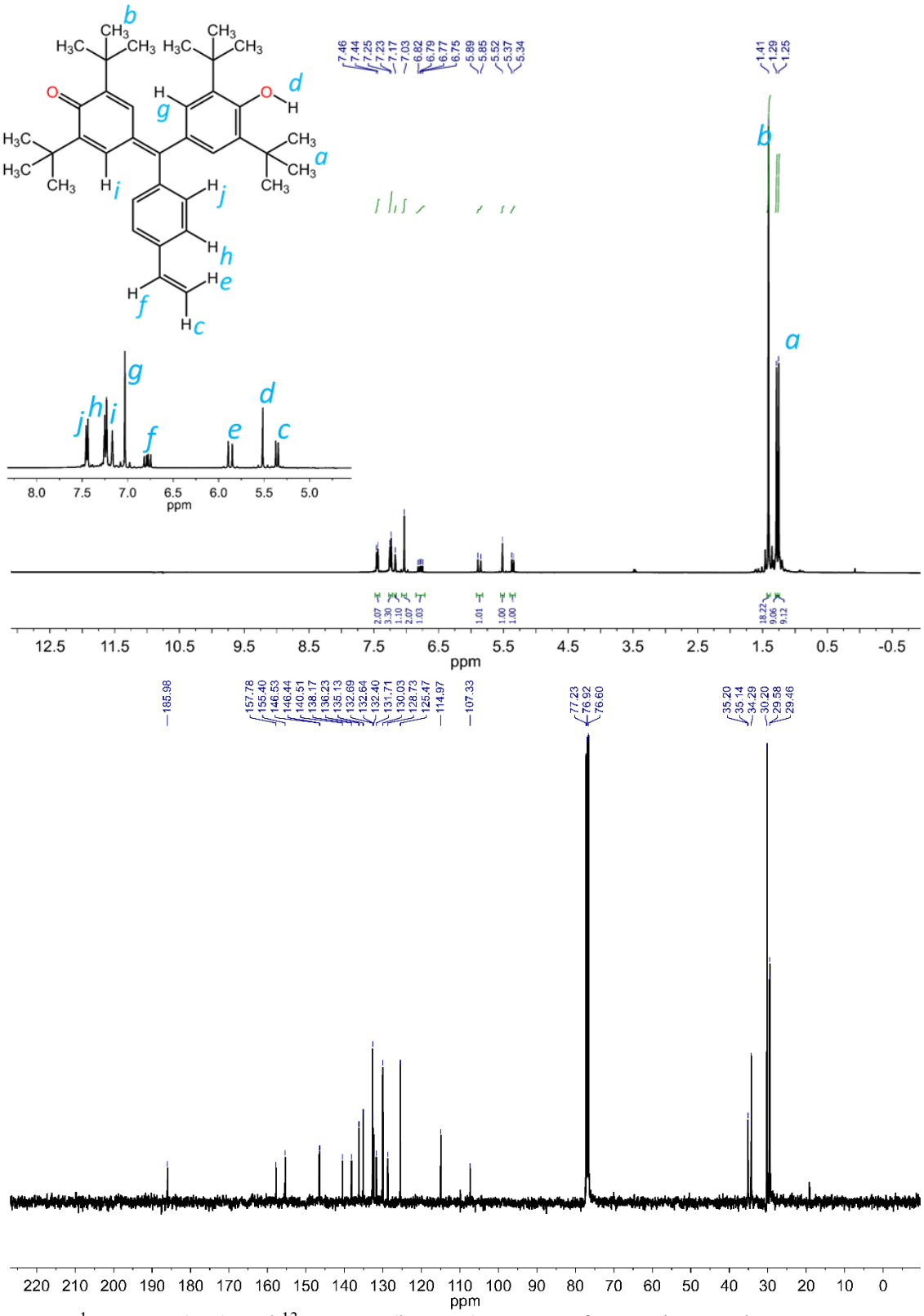

Figure S1: ^{1}H NMR (top) and ^{13}C NMR (bottom) spectra of GStH in $CDCl_3$.

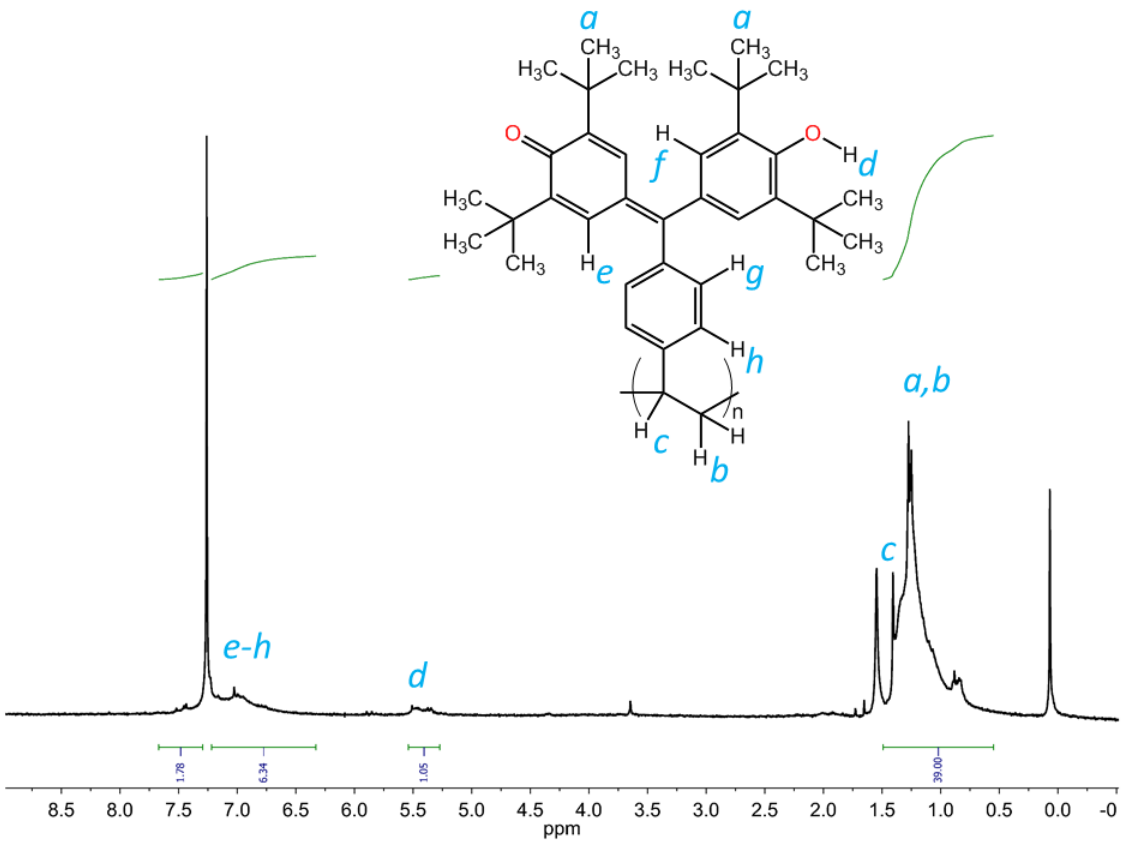

Figure S2: ^{1}H NMR spectrum of PGStH in $CDCl_3$.

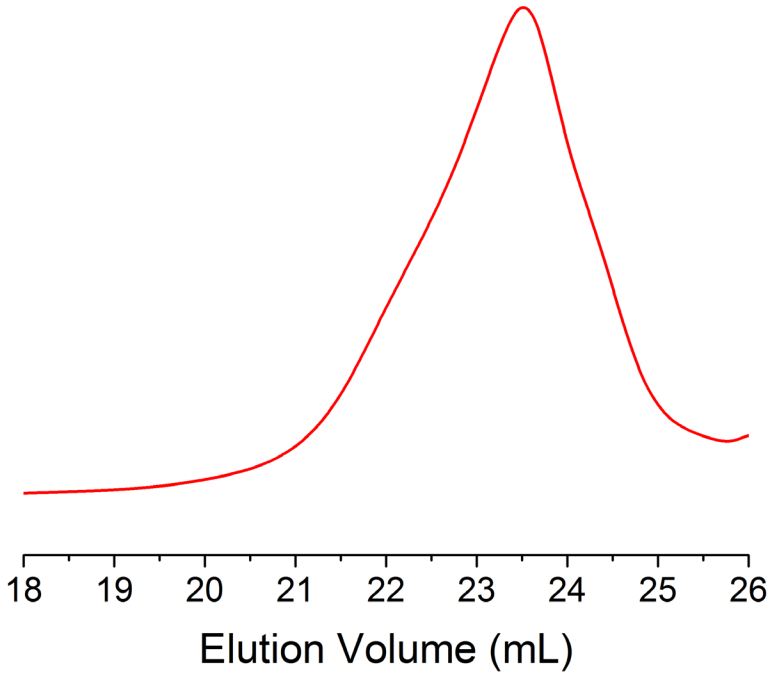

Figure S3: SEC trace demonstrating the macromolecular nature of the PGStH. The number-average molecular weight of PGStH was 4.1 kg mol^{-1}, and the dispersity was 1.22.

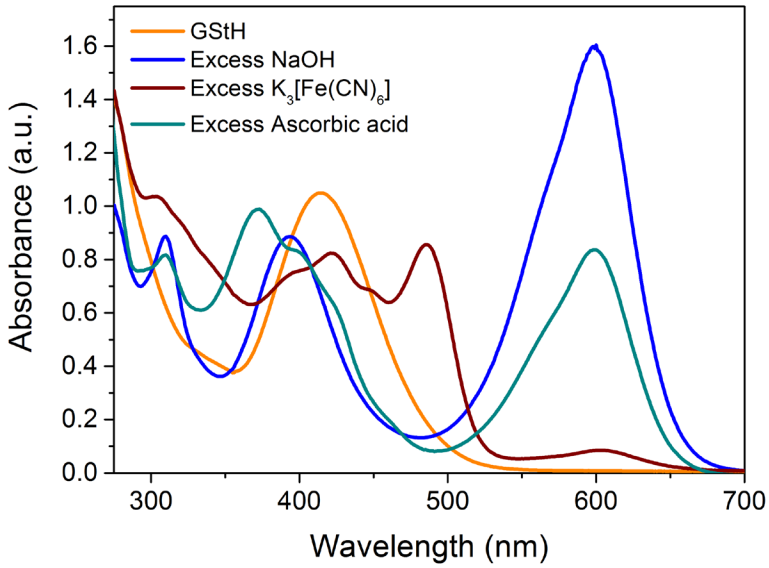

Figure S4: UV-Vis absorption spectra of GStH (0.1 mM) is shown (orange). The addition of excess NaOH (aq.) forms the conjugate base, GStB (blue). Further, the oxidation of GStB by $K_3[Fe(CN)_6]$ forms the radical species GSt with a clear absorption peak at 485 nm (brown). Addition of excess ascorbic acid regenerates the anionic species (GStB). The partial recovery observed in this process is due to the instability of GSt in alkaline media.

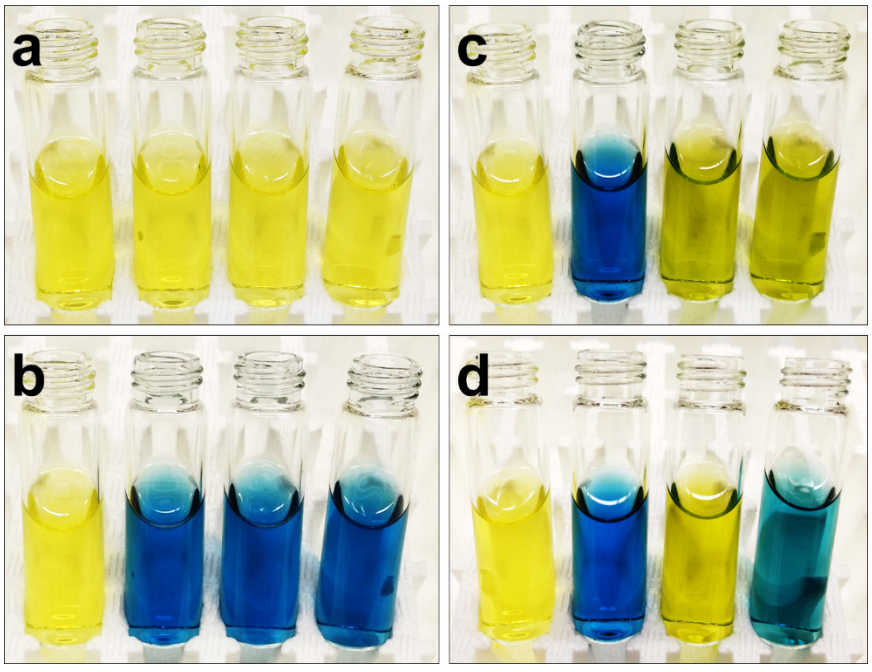

Figure S5: Digital photographs of the solutions described in the above graph. Panel (a) shows four different vials of the GStH solution. Panel (b) shows that the addition of excess NaOH to the last three samples results in a distinct color change due to the formation of GStB. Panel (c) shows that the further addition of $K_3[Fe(CN)_6]$ oxidizes the anions to the corresponding radical (GSt) in the last two vials. At last, as shown in panel (d), addition of a radical scavenger (ascorbic acid) partially regenerates the GStB species in solution.

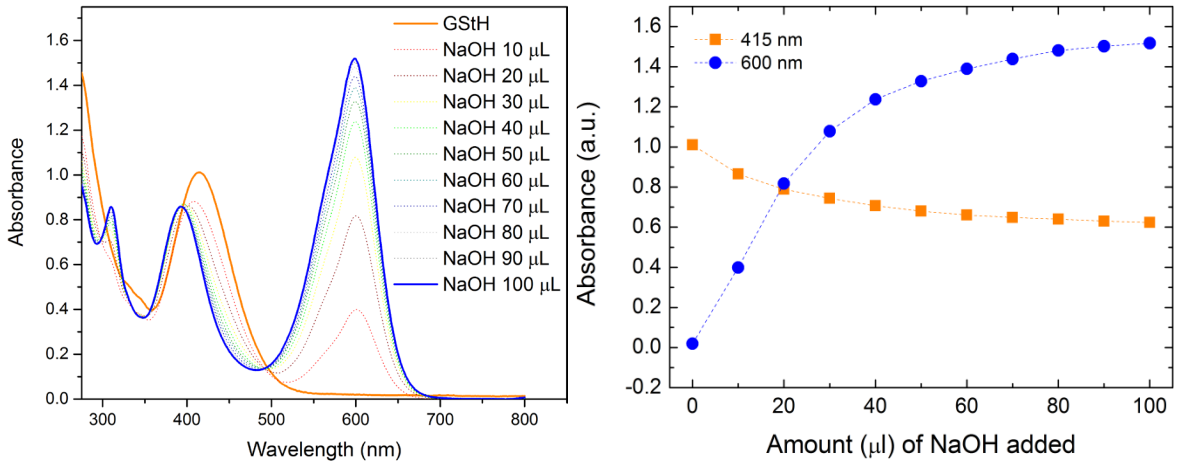

Figure S6: Changes in the absorption profile upon addition of NaOH (aq., 0.1 g mL^{-1}) to a 0.1 mM (1:9 THF-H_2O) solution of (3 mL) GStH (left). Also, the evolution of the peaks as a function of the amount of NaOH (aq.) added at 415 nm and 600 nm are shown (right).

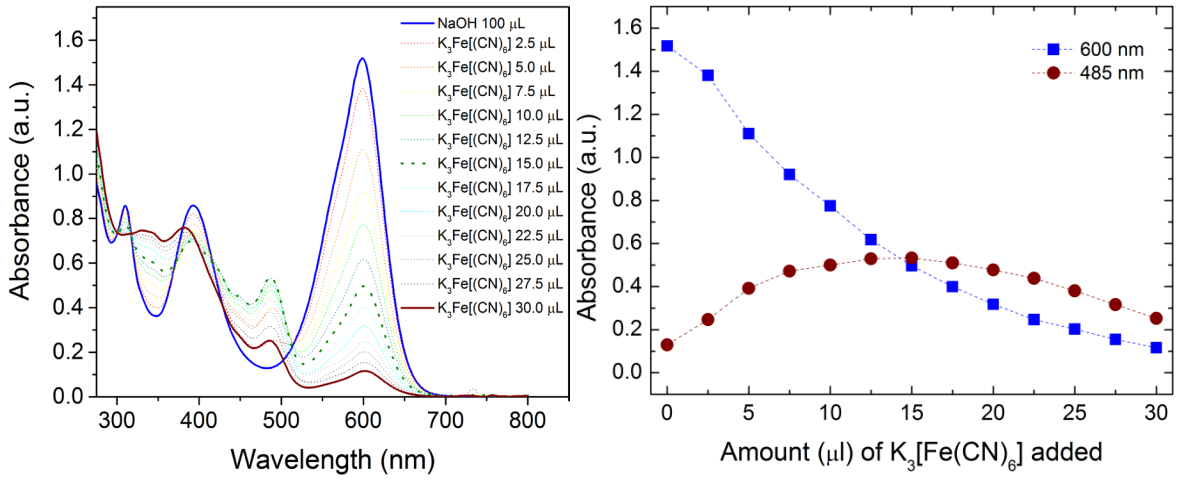

Figure S7: Changes in the absorption profile upon addition of $K_3[Fe(CN)_6]$ (aq., 10 mM) to a 0.1 mM (1:9 THF-H_2O) solution of (3 mL) GStB (left). Also, the evolution of the peaks at 485 nm and 600 nm as a function of the amount of $K_3[Fe(CN)_6]$ are shown (right).

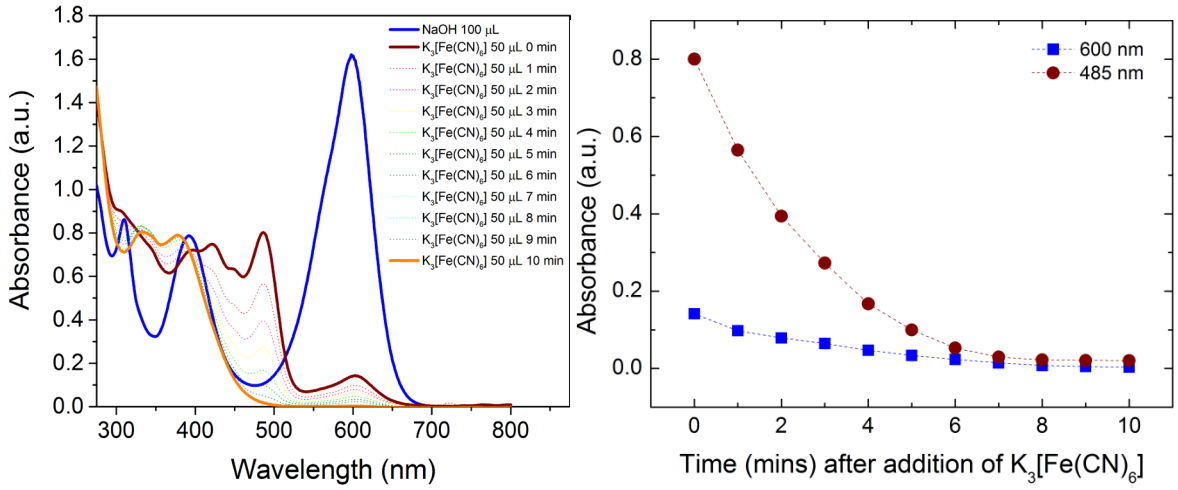

Figure S8: UV-Vis changes show decomposition of GSt, which was formed at once after addition of excess $K_3[Fe(CN)_6]$ to GStB. The evolution of the peaks at 485 nm and 600 nm are shown as a function of time after the addition of $K_3[Fe(CN)_6]$ (right).

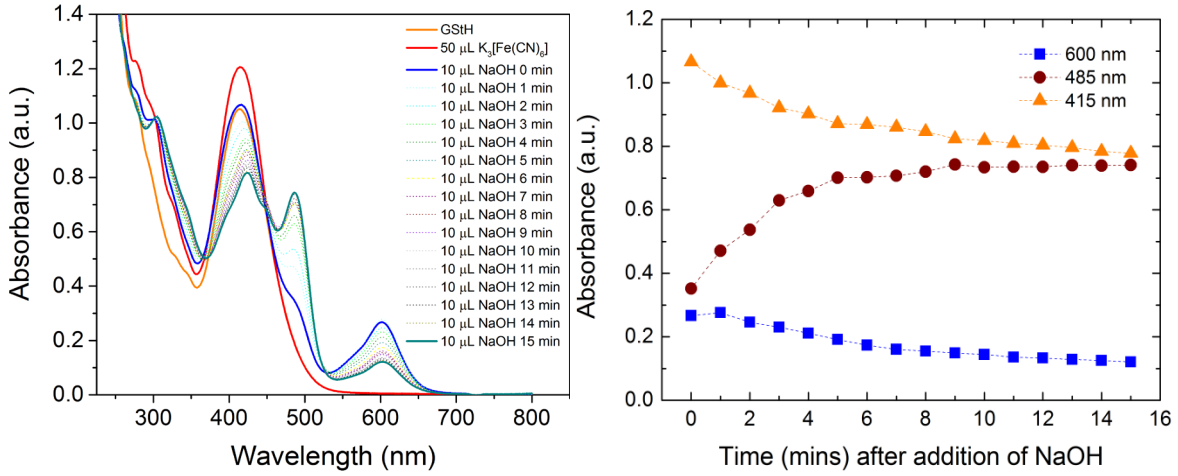

Figure S9: GStH does not show any reactivity towards the presence of $K_3[Fe(CN)_6]$ in 1:9 THF-H_2O mixture (left). After addition of a relatively smaller amount of NaOH (10 ul of 0.1 g/mL), the conversion starts resulting in steady formation of the radical species. The absorbances at 415 nm, 485 nm and 600 nm show that the peak at 600 nm slowly decay during the process (right).

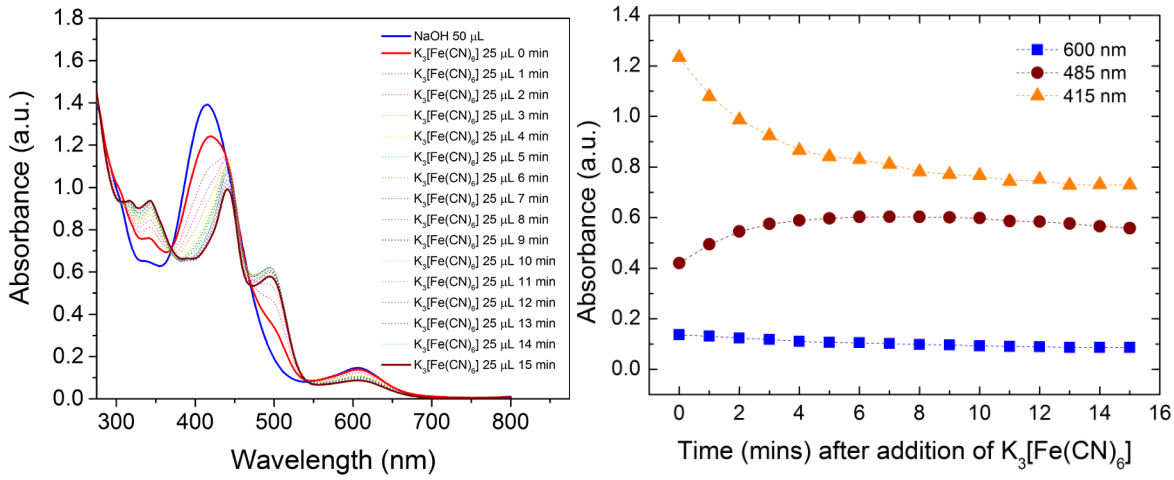

Figure S10: Changes in the absorption profile upon addition of $K_3[Fe(CN)_6]$ (aq., 10 mM) to a 0.1 mM (1:9 THF-H_2O) solution of (3 mL) PGStH (left) in presence of NaOH. Also, the evolution of the peaks at 485 nm and 600 nm as a function of time after the addition of $K_3[Fe(CN)_6$ are shown (right).

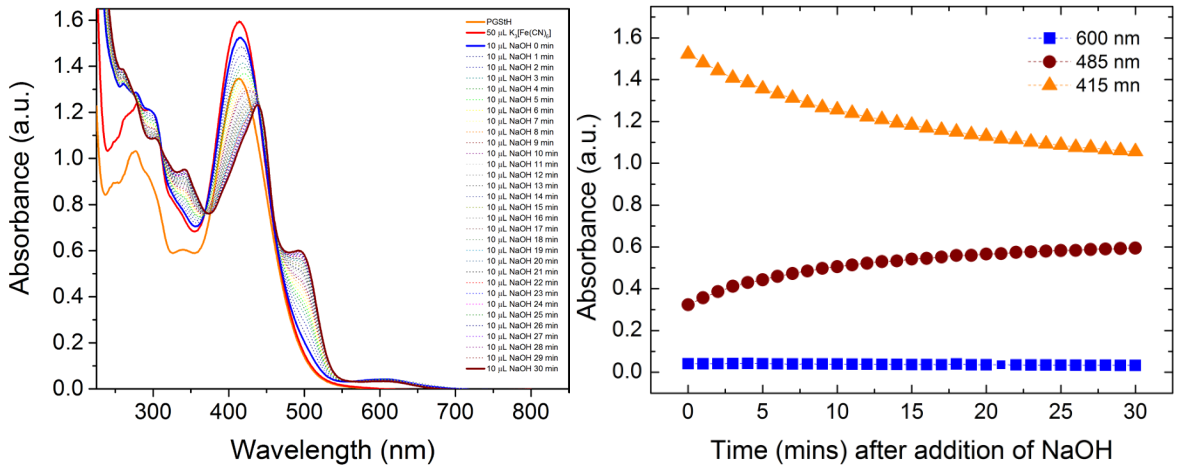

Figure S11: PGStH does not show any reactivity towards the presence of $K_3[Fe(CN)_6]$ in 1:9 THF-H_2O mixture (left). After addition of a relatively smaller amount of NaOH (10 ul of 0.1 g/mL), the conversion starts resulting in steady formation of the radical species. The absorbances at 415 nm, 485 nm and 600 nm show that the peak at 600 nm remain constant during the process (right).

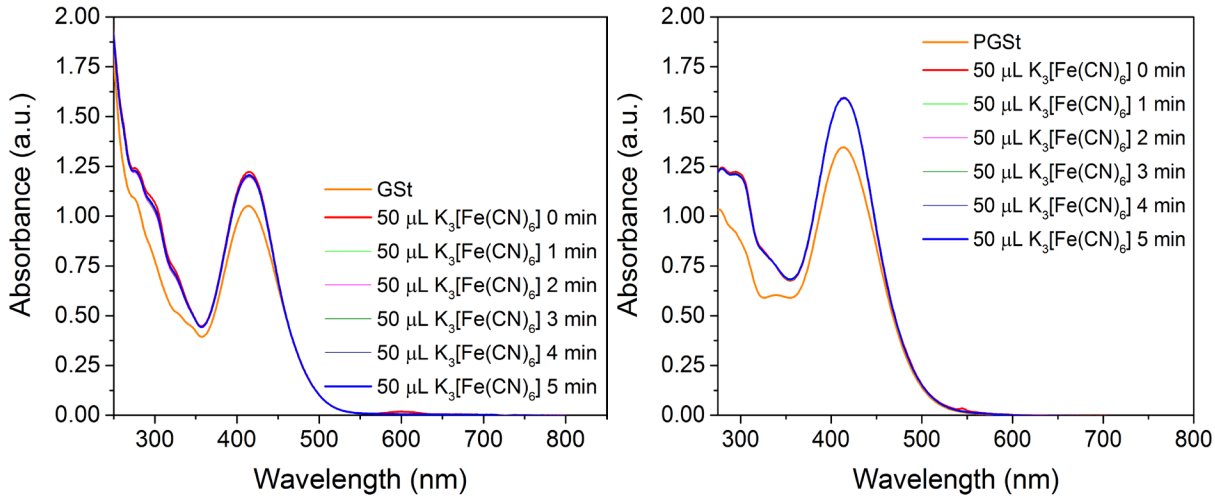

Figure S12: UV-Vis spectra of GStH (left) (0.1 mM, in 1:9 THF-H_2O) and PGStH (right) in the presence of excess amount of $K_3[Fe(CN)_6]$.

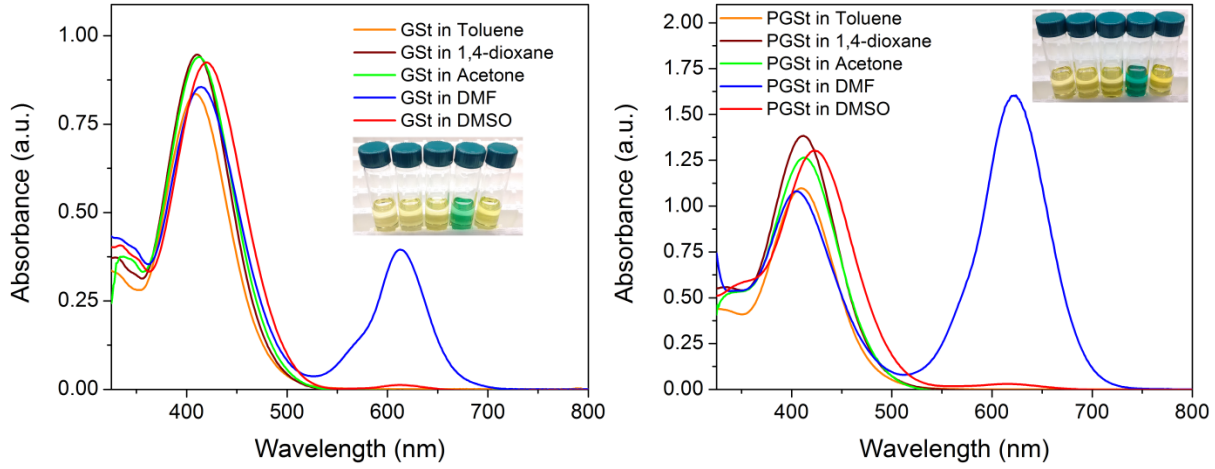

Figure S13: UV-Vis spectra of GStH (left) (0.1 mM) and PGStH (right) in different solvents. Inset shows digital photograph of the solutions respectively.

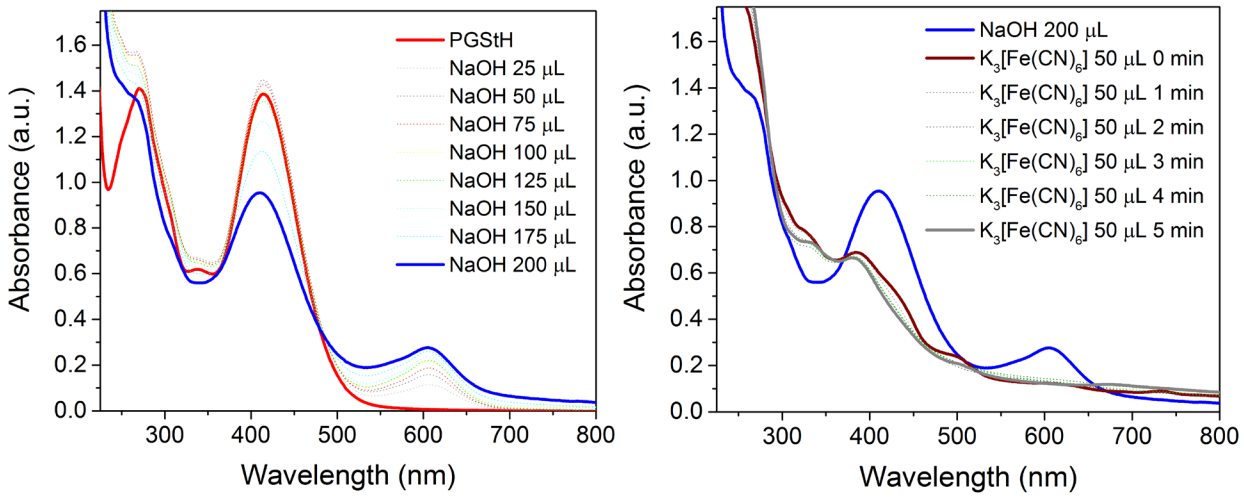

Figure S14: Changes in the UV-Vis spectra of PGStH (in 1:9 THF-Water) upon addition of excess of NaOH (aq, 0.1 g mL^{-1}) (left) following the addition of aq. $K_3[Fe(CN)_6]$ (right).

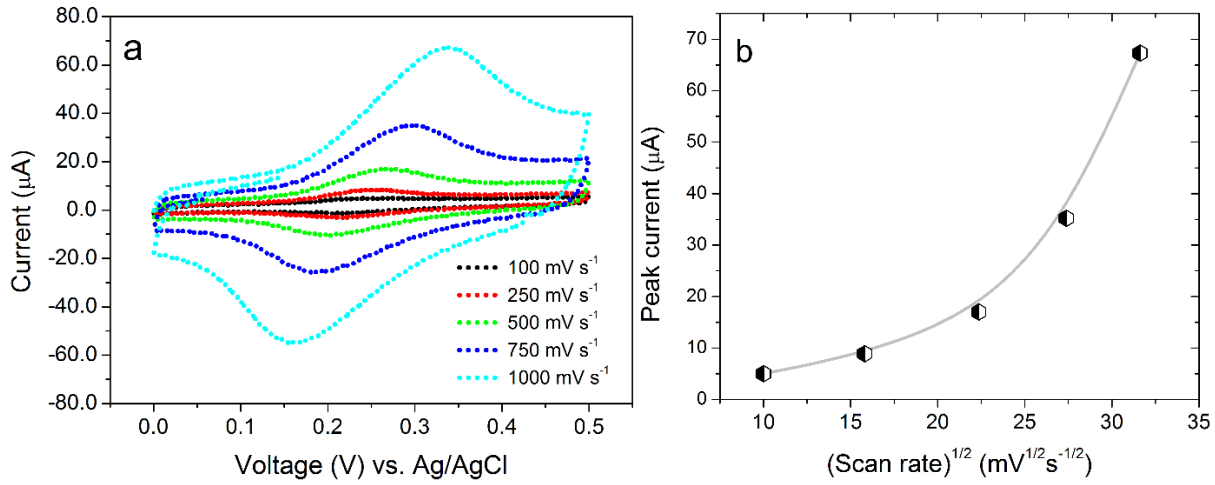

Figure S15: (a) Cyclic voltammogram of *in situ* prepared GSt in 300 ml of tetrahydrofuran (THF) {0.01 mM of GStB, with 1 mL of (0.1 g mL^{-1}) aqueous NaOH and 1 mL of 10 mM aqueous $K_3[Fe(CN)_6]$} solution with 5 g of tetrabutylammonium hexafluorophosphate added to solution in order to serve as the supporting electrolyte. The scan rate was varied between 0.1 V s^{-1} and 1.0 V s^{-1}. (b) The scan-rate dependence of the forward peak-current is shown. The non-linear feature of the graph is ascribed to the instability and reactivity of GSt in THF-H_2O media.

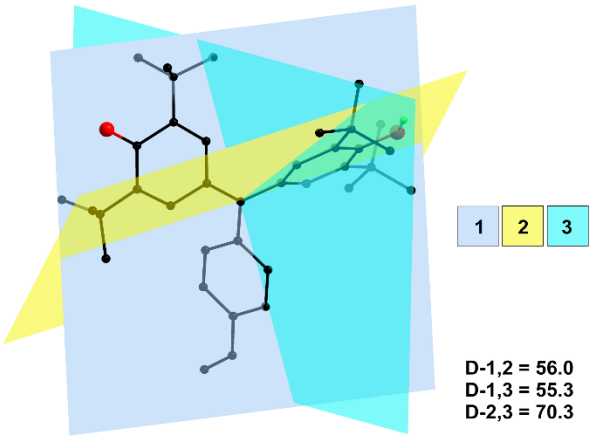

Figure S16: Dihedral arrangements of the three aromatic rings in GStH. D-i,j represents the angle between the planes i and j. As shown the arrangements of the two phenolic rings are not symmetric compared to the styryl moiety. The H atoms are omitted for clarity.

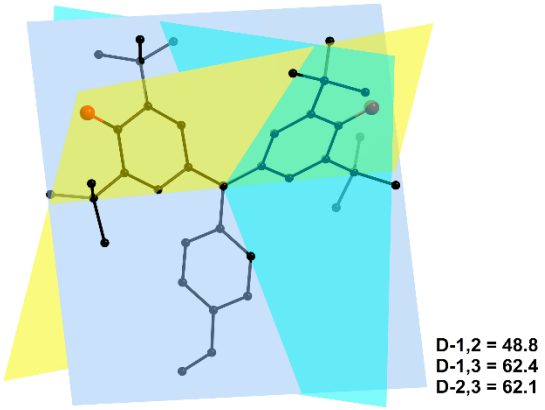

Figure S17: Dihedral arrangements of the three aromatic rings in GStB. As shown the arrangements of the two phenolic rings are symmetric compared to the styryl moiety. The H atoms are omitted for clarity.

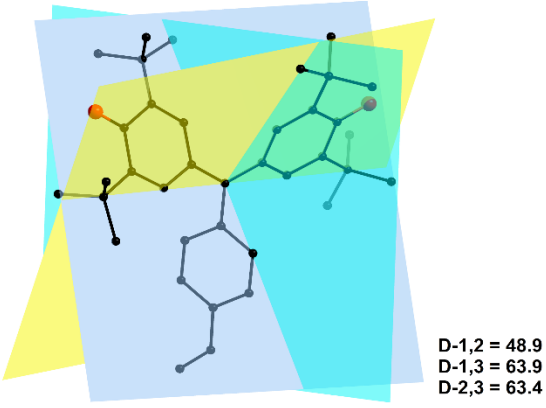

Figure S18: Dihedral arrangements of the three aromatic rings in GSt. As shown the arrangements of the two phenolic rings are symmetric compared to the styryl moiety. The H atoms are omitted for clarity.

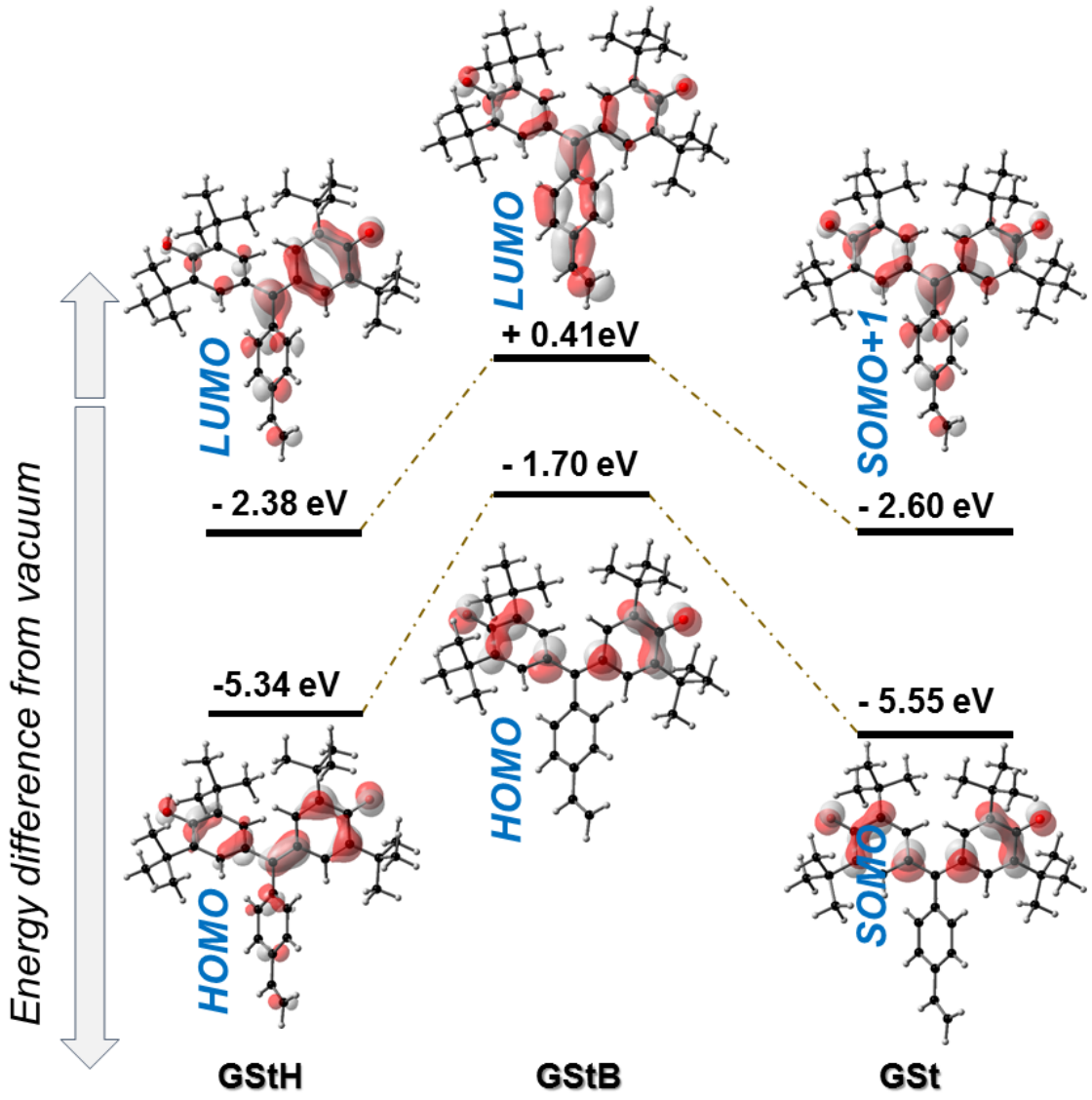

Figure S19: DFT obtained frontier molecular orbitals (FMOs) of the compounds. Although qualitative, the results clearly demonstrate the diminished band-gap in GStB compared to GStH, which can be correlated to the increased conjugation in the system. The FMOs are mostly concentrated on the phenolic moieties except for the LUMO of GStB, which is delocalized throughout the molecular backbone. The figures have been visualized using GaussView 5.0 software package, using a isocontour value of 0.04 units for the molecular orbitals.

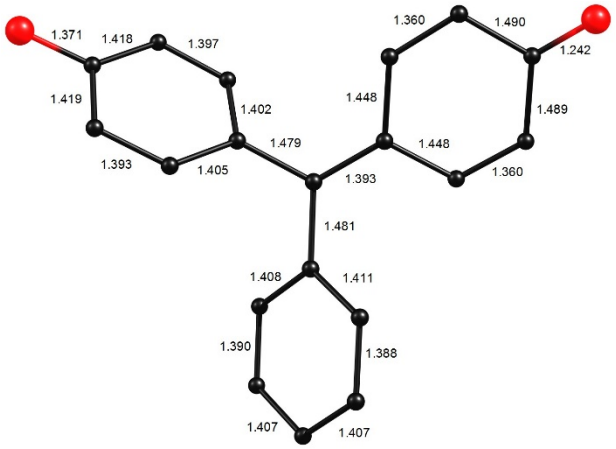

Figure S20: DFT obtained important bond lengths (Å) of the conjugated backbone of GStH.

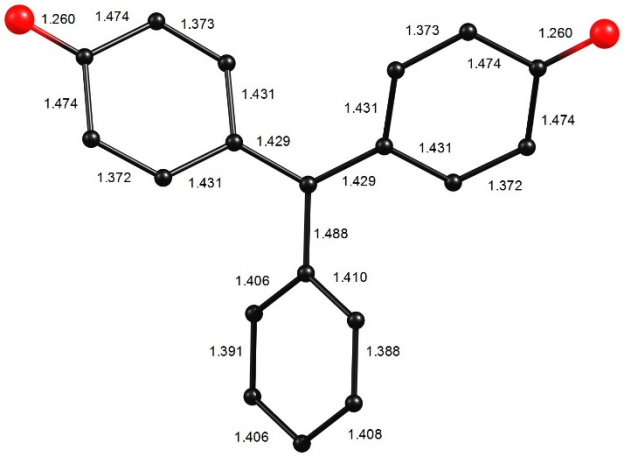

Figure S21: DFT obtained important bond lengths (Å) of the conjugated backbone of GStB.

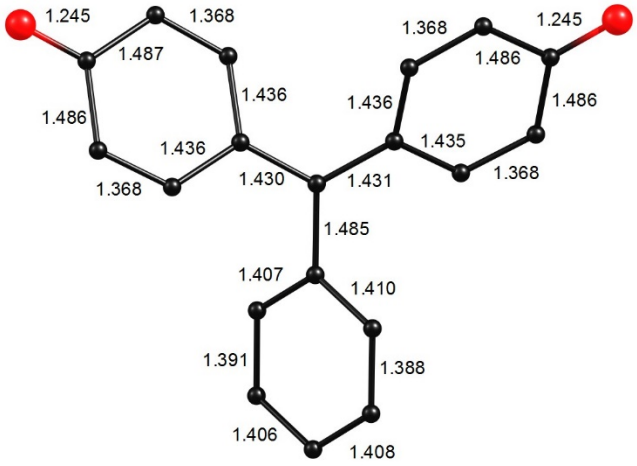

Figure S22: DFT obtained important bond lengths (Å) of the conjugated backbone of GSt.

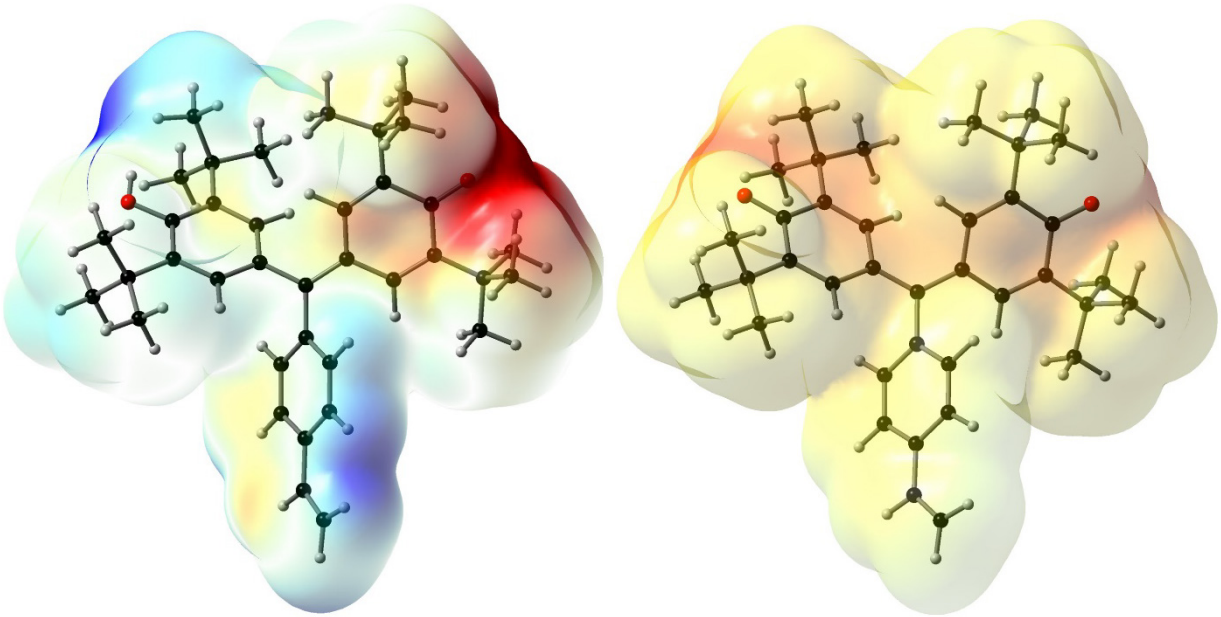

Figure S23: Electrostatic potential (ESP) surface (isovalue = 0.0004) of GStH (left, ± 0.02) and GStB (right, ± 0.15). The positive potential are shown by the blue and green pattern whereas the negative potential is depicted by yellow and red patterns. The symmetrical ESP surface of GStB shows the anionic charge throughout the molecular backbone.

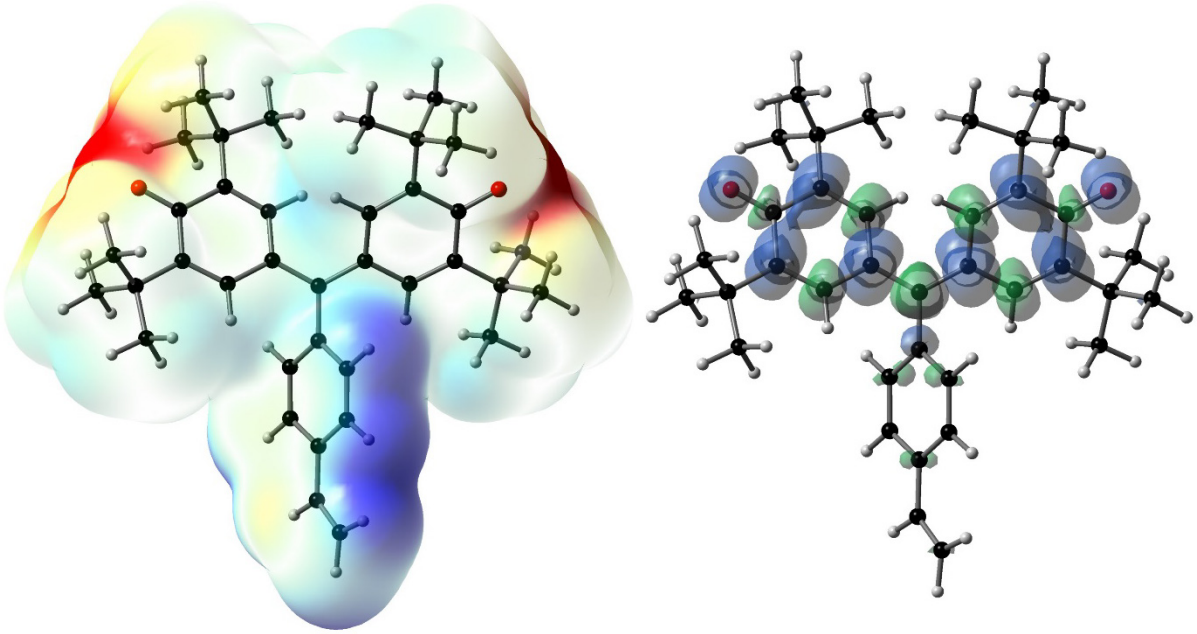

Figure S24: Electrostatic potential (ESP) surface (isovalue = 0.0004) of GSt (left, ± 0.02). The positive potential are shown by the blue and green pattern whereas the negative potential is depicted by yellow and red patterns. The spin density plot of GSt (right, isovalue = 0.04) shows that the spin is mostly localised in the two phenolic units, similar to a galvinoxyl radical.

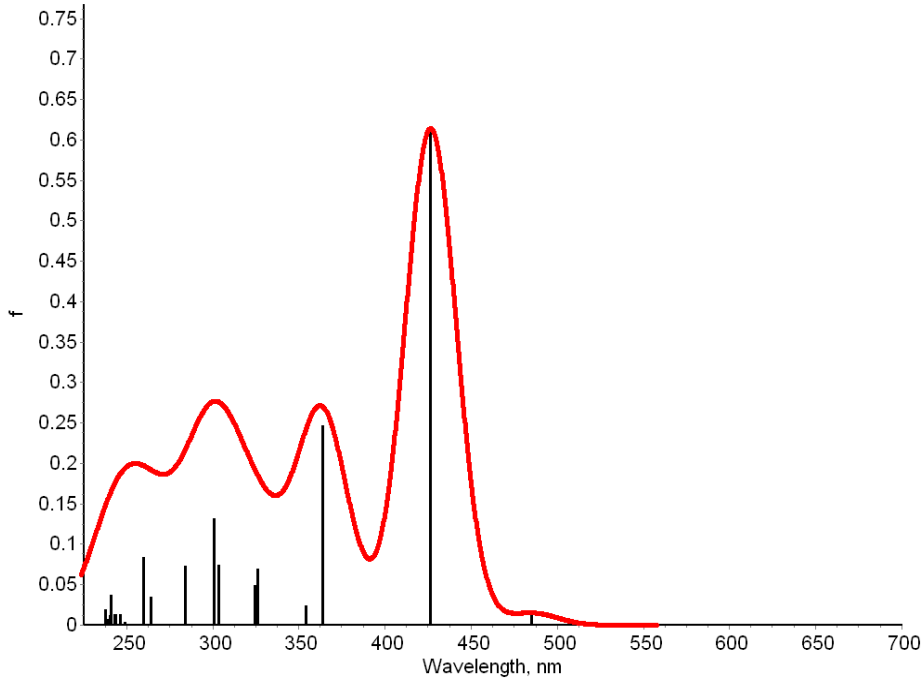

Figure S25: TD-DFT (B3LYP/6-31G*, nstates = 20) simulated UV-Vis absorption spectrum of GStH.

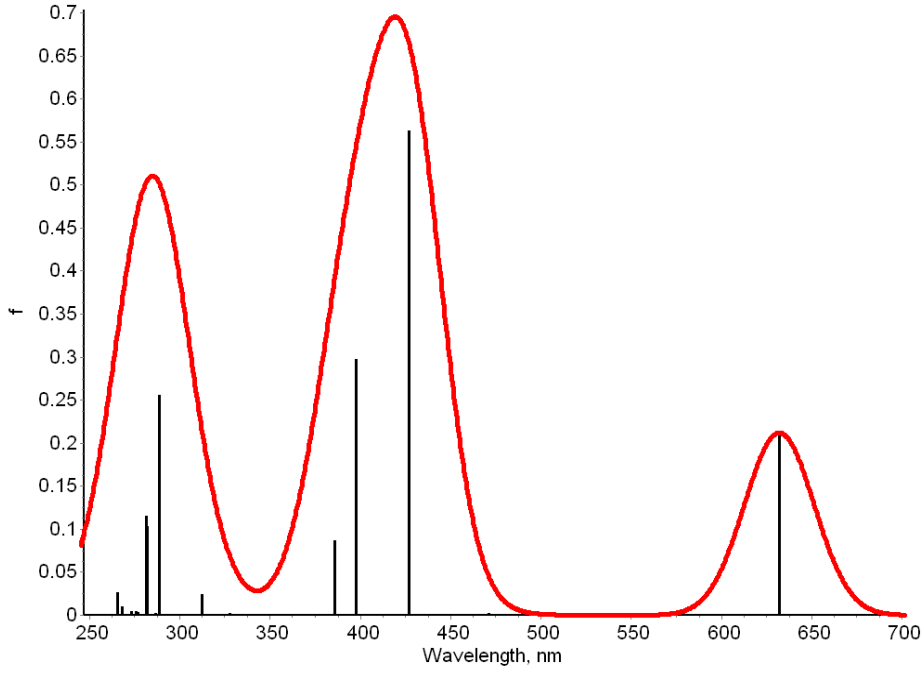

Figure S26: TD-DFT (B3LYP/6-31G*, nstates = 20) simulated UV-Vis absorption spectrum of GStB.

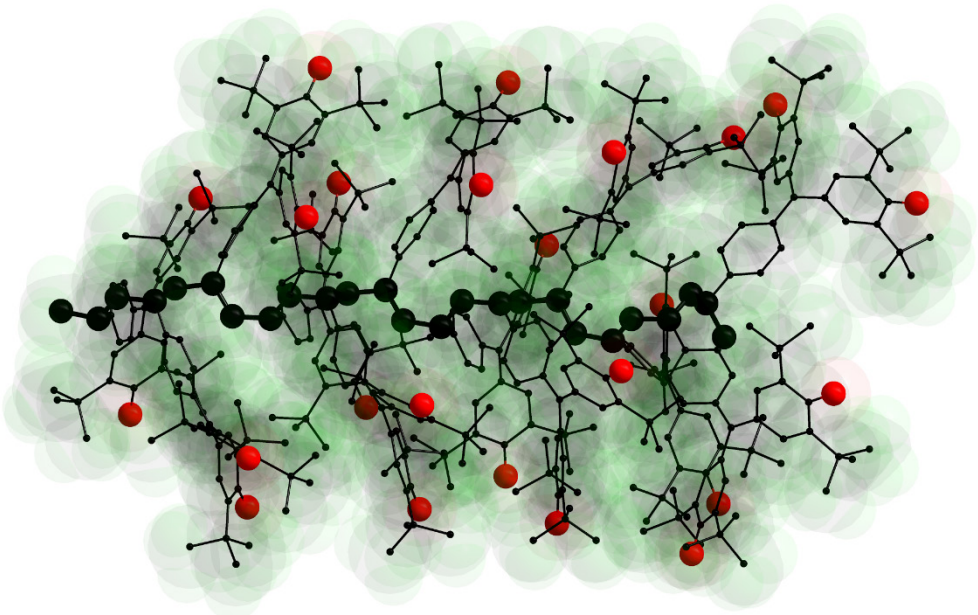

Figure S27: Side view of the molecular mechanics obtained structure of a PGSt (with 12 repeating units). The main polymer backbone and the peripheral oxygen atoms are shown as bigger spheres. The space-fill model is superimposed to ease the visualization of the polymer. (C = black, H = green transparent spheres, O = red)

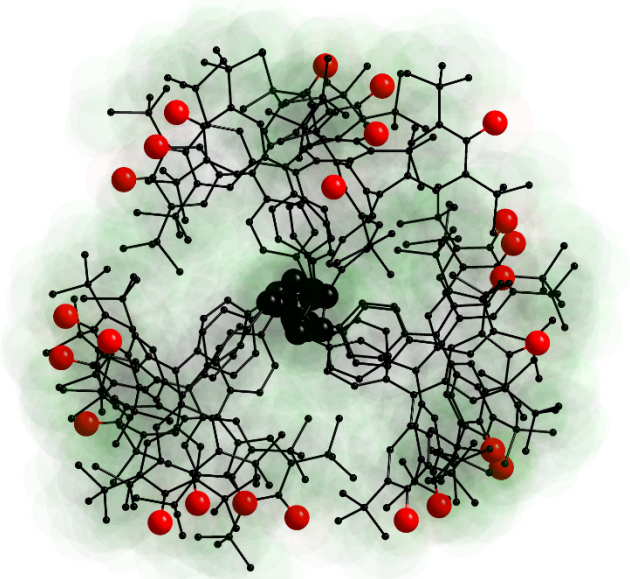

Figure S28: Top view of the molecular mechanics obtained structure of a PGSt (with 12 repeating units). The main polymer backbone and the peripheral oxygen atoms are shown as bigger spheres. The space-fill model is superimposed to ease the visualization of the polymer. (C = black, H = green transparent spheres, O = red)

Table S1: DFT (B3LYP/6-31G*) obtained geometry coordinates of GStH.

Centre Number	Atomic Number	Coordinates (Angstroms)		
		X	Y	Z
1	6	1.211085	0.171632	-0.0933
2	6	2.283329	0.749118	0.607383
3	6	3.569898	0.214145	0.593712
4	6	3.775127	-0.94611	-0.19669
5	6	2.737088	-1.55373	-0.94795
6	6	1.470262	-0.97037	-0.86503
7	1	2.081663	1.633987	1.195999
8	1	0.650739	-1.3859	-1.43539
9	6	-0.19437	2.253968	-0.17489
10	6	0.624001	2.940227	-1.09192
11	6	-1.03507	3.028299	0.653059
12	6	0.575485	4.324984	-1.1975
13	1	1.288415	2.374705	-1.73796
14	6	-1.06962	4.412415	0.555333
15	1	-1.64745	2.528896	1.397397
16	6	-0.26906	5.096266	-0.3786
17	1	1.205214	4.826473	-1.92883
18	1	-1.7219	4.969647	1.221185
19	6	-1.28997	0.009845	0.078793
20	6	-2.59609	0.525778	-0.27547
21	6	-1.24027	-1.34886	0.577926
22	6	-3.74244	-0.20013	-0.18262
23	1	-2.62675	1.522617	-0.69487
24	6	-2.34191	-2.12825	0.74763
25	1	-0.27053	-1.71346	0.889137
26	6	-3.67379	-1.58628	0.358086
27	6	-0.13682	0.779213	-0.05558
28	6	-2.25987	-3.5424	1.350552
29	6	-5.10412	0.35927	-0.63227
30	6	-0.81364	-3.93065	1.716821
31	1	-0.38413	-3.26243	2.47243
32	1	-0.8069	-4.94431	2.132968
33	1	-0.15052	-3.93028	0.842819
34	6	-2.7809	-4.5814	0.325976
35	1	-2.71544	-5.59033	0.752445
36	1	-3.81924	-4.3817	0.059197
37	1	-2.17431	-4.56401	-0.58826
38	6	-3.106	-3.61848	2.645957
39	1	-2.73324	-2.9089	3.394924

40	1	-4.15431	-3.39519	2.444737
41	1	-3.03904	-4.62568	3.076314
42	6	-5.70131	-0.5289	-1.75219
43	1	-5.84809	-1.55319	-1.40764
44	1	-6.67067	-0.12455	-2.06967
45	1	-5.04165	-0.54391	-2.62869
46	6	-4.98403	1.792103	-1.18851
47	1	-4.5961	2.495952	-0.44262
48	1	-4.33794	1.839966	-2.07323
49	1	-5.97663	2.146261	-1.48834
50	6	-6.07661	0.402994	0.573423
51	1	-7.04475	0.811125	0.256664
52	1	-6.23641	-0.59402	0.985511
53	1	-5.68308	1.051387	1.366095
54	6	4.714348	0.864996	1.406279
55	6	5.845627	1.338238	0.459377
56	1	6.644975	1.809088	1.044712
57	1	6.278884	0.511717	-0.10584
58	1	5.468695	2.083084	-0.25175
59	6	4.226937	2.104482	2.186469
60	1	3.838457	2.886552	1.524395
61	1	3.449654	1.853785	2.917357
62	1	5.070325	2.532287	2.739606
63	6	5.274826	-0.13619	2.447049
64	1	5.69728	-1.0238	1.973984
65	1	6.063626	0.346324	3.037127
66	1	4.486487	-0.45508	3.139159
67	6	2.973412	-2.80003	-1.84078
68	6	3.417827	-4.01776	-0.98489
69	1	3.574332	-4.89158	-1.62778
70	1	4.342558	-3.86819	-0.41585
71	1	2.641606	-4.26803	-0.25391
72	6	4.008152	-2.49281	-2.95791
73	1	4.991247	-2.17628	-2.59373
74	1	4.162705	-3.38119	-3.58108
75	1	3.639327	-1.68727	-3.60191
76	6	1.683092	-3.24021	-2.56565
77	1	0.889896	-3.51782	-1.86361
78	1	1.29833	-2.45814	-3.2285
79	1	1.898627	-4.11893	-3.18319
80	6	-0.26834	6.558281	-0.52868
81	1	0.404882	6.932882	-1.2997
82	6	-0.98926	7.449062	0.165

83	1	-1.68371	7.1649	0.950951
84	1	-0.90434	8.512233	-0.03731
85	8	5.052388	-1.44484	-0.20395
86	1	5.085023	-2.24668	-0.74062
87	8	-4.70088	-2.27262	0.483294

Table S2: DFT (B3LYP/6-31G*) obtained geometry coordinates of GStB.

Centre Number	**Atomic Number**	**Coordinates (Angstroms)**		
		X	**Y**	**Z**
1	6	1.26993	0.118634	-0.10375
2	6	2.455159	0.774297	0.359262
3	6	3.700768	0.199013	0.33359
4	6	3.861854	-1.15446	-0.22763
5	6	2.657569	-1.81762	-0.75873
6	6	1.441333	-1.18882	-0.65995
7	1	2.332594	1.757404	0.79782
8	1	0.558182	-1.65766	-1.07629
9	6	-0.06831	2.232876	-0.06179
10	6	0.701371	2.976334	-0.97444
11	6	-0.8965	2.95327	0.823753
12	6	0.641088	4.365988	-1.00137
13	1	1.341408	2.448053	-1.67399
14	6	-0.94878	4.340512	0.802317
15	1	-1.49372	2.402178	1.543417
16	6	-0.18092	5.082854	-0.11468
17	1	1.239723	4.912921	-1.72737
18	1	-1.59213	4.854891	1.511178
19	6	-1.24204	0.026541	0.069434
20	6	-2.47138	0.568921	-0.4237
21	6	-1.31569	-1.26516	0.681011
22	6	-3.66884	-0.09994	-0.3784
23	1	-2.42188	1.539896	-0.90198
24	6	-2.48032	-1.9817	0.802685
25	1	-0.40173	-1.64669	1.119481
26	6	-3.72814	-1.43768	0.238218
27	6	-0.01167	0.746105	-0.03039
28	6	-2.52506	-3.33711	1.53551
29	6	-4.95835	0.505166	-0.96728
30	6	-1.15335	-3.74105	2.111067
31	1	-0.78492	-3.01425	2.844952
32	1	-1.2443	-4.70853	2.620575

33	1	-0.39004	-3.84998	1.331548
34	6	-2.96853	-4.44758	0.550769
35	1	-3.02419	-5.41603	1.067685
36	1	-3.94716	-4.21239	0.12944
37	1	-2.24618	-4.54568	-0.26949
38	6	-3.52347	-3.2698	2.717369
39	1	-3.20152	-2.51969	3.451159
40	1	-4.52002	-3.00586	2.360714
41	1	-3.57235	-4.24126	3.228899
42	6	-5.50554	-0.40979	-2.09033
43	1	-5.70305	-1.40974	-1.70159
44	1	-6.43629	0.005391	-2.50229
45	1	-4.78031	-0.48815	-2.91028
46	6	-4.72881	1.903256	-1.57443
47	1	-4.35925	2.620848	-0.83203
48	1	-4.01484	1.879473	-2.40648
49	1	-5.67833	2.290305	-1.96531
50	6	-6.02624	0.647949	0.14577
51	1	-6.95816	1.056533	-0.26981
52	1	-6.23345	-0.32286	0.598274
53	1	-5.67757	1.334451	0.928023
54	6	4.941505	0.928357	0.885235
55	6	5.987422	1.108677	-0.24314
56	1	6.884885	1.6103	0.145422
57	1	6.271026	0.138728	-0.65424
58	1	5.579182	1.728503	-1.05181
59	6	4.604228	2.327921	1.436471
60	1	4.175659	2.982456	0.668024
61	1	3.897766	2.281886	2.273973
62	1	5.521484	2.805232	1.803988
63	6	5.568584	0.107966	2.039298
64	1	5.841807	-0.88892	1.690491
65	1	6.466728	0.612868	2.422224
66	1	4.85875	0.007411	2.870248
67	6	2.804604	-3.19496	-1.43522
68	6	3.344886	-4.22467	-0.41207
69	1	3.475114	-5.20546	-0.8908
70	1	4.304214	-3.89327	-0.01188
71	1	2.639428	-4.34788	0.419446
72	6	3.783825	-3.09638	-2.63102
73	1	4.758311	-2.73626	-2.29809
74	1	3.908767	-4.08141	-3.10219
75	1	3.394342	-2.4074	-3.39149

76	6	1.46446	-3.73075	-1.97638
77	1	0.72003	-3.86382	-1.18261
78	1	1.032755	-3.06904	-2.73687
79	1	1.627222	-4.70989	-2.444
80	6	-0.19878	6.550243	-0.18562
81	1	0.448939	6.969995	-0.95649
82	6	-0.90203	7.403147	0.572394
83	1	-1.57074	7.074416	1.363388
84	1	-0.82758	8.476057	0.42106
85	8	4.989836	-1.71409	-0.2669
86	8	-4.80905	-2.08235	0.294751

Table S3: DFT (B3LYP/6-31G*) obtained geometry coordinates of GSt.

Centre Number	**Atomic Number**	**Coordinates (Angstroms)**		
		X	**Y**	**Z**
1	6	1.266962	0.102052	-0.09568
2	6	2.449777	0.780272	0.353357
3	6	3.693669	0.212481	0.329124
4	6	3.838311	-1.15531	-0.23332
5	6	2.631239	-1.83973	-0.76701
6	6	1.421746	-1.21084	-0.65667
7	1	2.317664	1.765346	0.7803
8	1	0.536006	-1.67628	-1.06814
9	6	-0.06511	2.22622	-0.06399
10	6	0.675582	2.963673	-1.00531
11	6	-0.86381	2.945704	0.848776
12	6	0.61421	4.352666	-1.03323
13	1	1.288146	2.437901	-1.73151
14	6	-0.9129	4.332497	0.826412
15	1	-1.4362	2.401985	1.594381
16	6	-0.17494	5.071333	-0.11802
17	1	1.186231	4.896694	-1.78107
18	1	-1.53153	4.8485	1.554461
19	6	-1.23885	0.014005	0.058715
20	6	-2.46336	0.581032	-0.42927
21	6	-1.30175	-1.27678	0.683687
22	6	-3.66259	-0.07549	-0.38488
23	1	-2.39941	1.551788	-0.90227
24	6	-2.46306	-1.98739	0.818054
25	1	-0.38788	-1.65543	1.121887
26	6	-3.71137	-1.42121	0.243214

27	6	-0.0101	0.742323	-0.03228
28	6	-2.51687	-3.33751	1.551245
29	6	-4.94724	0.527437	-0.97593
30	6	-1.14378	-3.73577	2.128985
31	1	-0.77597	-3.00657	2.860451
32	1	-1.23689	-4.69812	2.643852
33	1	-0.38153	-3.8555	1.349901
34	6	-2.95615	-4.44999	0.564673
35	1	-2.98032	-5.41574	1.084321
36	1	-3.94779	-4.24794	0.15796
37	1	-2.2464	-4.53565	-0.26733
38	6	-3.5167	-3.26263	2.733037
39	1	-3.21113	-2.49413	3.453584
40	1	-4.52532	-3.0356	2.386175
41	1	-3.53668	-4.22485	3.258957
42	6	-5.48962	-0.38533	-2.1048
43	1	-5.73185	-1.37942	-1.72742
44	1	-6.39719	0.057167	-2.53358
45	1	-4.75335	-0.48565	-2.91158
46	6	-4.70218	1.925122	-1.5791
47	1	-4.33556	2.640337	-0.83338
48	1	-3.98723	1.898115	-2.40981
49	1	-5.64638	2.31668	-1.9732
50	6	-6.01703	0.67579	0.136453
51	1	-6.92633	1.122144	-0.28418
52	1	-6.27272	-0.29132	0.570899
53	1	-5.65897	1.336465	0.935518
54	6	4.933948	0.937871	0.875469
55	6	5.980375	1.111161	-0.25546
56	1	6.856067	1.64565	0.132465
57	1	6.305855	0.145566	-0.64428
58	1	5.567068	1.701833	-1.08222
59	6	4.588646	2.34114	1.413336
60	1	4.164195	2.989569	0.637883
61	1	3.883275	2.301081	2.251662
62	1	5.503292	2.821284	1.778089
63	6	5.554509	0.125279	2.040212
64	1	5.865838	-0.866	1.708908
65	1	6.431242	0.654742	2.432804
66	1	4.836486	0.011698	2.861568
67	6	2.780248	-3.21582	-1.43618
68	6	3.314499	-4.24392	-0.40614
69	1	3.407433	-5.22813	-0.88145

70	1	4.291714	-3.94715	-0.02366
71	1	2.622353	-4.34473	0.438898
72	6	3.758406	-3.12013	-2.63463
73	1	4.749879	-2.79887	-2.31354
74	1	3.848399	-4.10183	-3.11542
75	1	3.385736	-2.41295	-3.38573
76	6	1.435272	-3.74416	-1.97423
77	1	0.693739	-3.88077	-1.17823
78	1	1.005053	-3.08249	-2.73528
79	1	1.595206	-4.72152	-2.4423
80	6	-0.19263	6.539601	-0.18963
81	1	0.406002	6.960236	-0.99732
82	6	-0.84763	7.384827	0.616835
83	1	-1.46251	7.052497	1.44881
84	1	-0.78513	8.458108	0.466823
85	8	4.949769	-1.71552	-0.26147
86	8	-4.77864	-2.06093	0.291132

References

[1] T. Suga, H. Ohshiro, S. Sugita, K. Oyaizu, H. Nishide, *Adv. Mater.*, 2009, **21**, 1627-1630.

[2] Gaussian 09, Revision D.01, M. J. Frisch, G. W. Trucks, H. B. Schlegel, G. E. Scuseria, M. A. Robb, J. R. Cheeseman, G. Scalmani, V. Barone, B. Mennucci, G. A. Petersson, H. Nakatsuji, M. Caricato, X. Li, H. P. Hratchian, A. F. Izmaylov, J. Bloino, G. Zheng, J. L. Sonnenberg, M. Hada, M. Ehara, K. Toyota, R. Fukuda, J. Hasegawa, M. Ishida, T. Nakajima, Y. Honda, O. Kitao, H. Nakai, T. Vreven, J. A. Montgomery, Jr., J. E. Peralta, F. Ogliaro, M. Bearpark, J. J. Heyd, E. Brothers, K. N. Kudin, V. N. Staroverov, T. Keith, R. Kobayashi, J. Normand, K. Raghavachari, A. Rendell, J. C. Burant, S. S. Iyengar, J. Tomasi, M. Cossi, N. Rega, J. M. Millam, M. Klene, J. E. Knox, J. B. Cross, V. Bakken, C. Adamo, J. Jaramillo, R. Gomperts, R. E. Stratmann, O. Yazyev, A. J. Austin, R. Cammi, C. Pomelli, J. W. Ochterski, R. L. Martin, K. Morokuma, V. G. Zakrzewski, G. A. Voth, P. Salvador, J. J. Dannenberg, S. Dapprich, A. D. Daniels, O. Farkas, J. B. Foresman, J. V. Ortiz, J. Cioslowski, and D. J. Fox, Gaussian, Inc., Wallingford CT, 2013.